High-Resolution Infrared Absorption Spectroscopy of C_{60} Molecules and Clusters in Parahydrogen Solids†

Norihito Sogoshi, Yoshiyasu Kato, Tomonari Wakabayashi, and Takamasa Momose*,‡

Department of Chemistry, Graduate School of Science, Kyoto University, and Japan Science and Technology Corporation (JST), Kyoto 606-8502, Japan

Simon Tam, Michelle E. DeRose, and Mario E. Fajardo*,§

Propulsion Directorate, U.S. Air Force Research Laboratory, AFRL/PRSP, Bldg. 8451, Edwards AFB, California 93524-7680

Received: November 1, 1999; In Final Form: February 1, 2000

We report the isolation of C_{60} molecules in cryogenic parahydrogen (pH_2) solids by the rapid vapor deposition method. New theoretical simulations of rovibrational spectra for low-temperature isolated $^{12}C_{60}$ molecules, including boson-exchange symmetry restrictions on the rotational levels, predict a characteristic "null gap" and unequal rotational line spacings for low-J values. High-resolution IR absorption spectra of the C_{60}/pH_2 samples failed to show rotationally resolved features, and in fact suggest that the majority of the C_{60} molecules are not rotating. However, spectra of the $F_{1u}(1)$ vibrational mode near 530 cm^{-1} show line widths of ≈0.2 cm^{-1} fwhm, the sharpest IR absorption bands for C_{60} reported to date. Visible absorption spectra also show sharp features in the ≈600 nm region, supporting our contention of well-isolated C_{60} molecules. The C_{60} molecules appear to stabilize the pH_2 solid, inhibiting the fcc to hcp conversion which usually occurs upon annealing of rapid vapor deposited pH_2 solids to $T \approx 5$ K. We also report surprisingly strong C_{60}-induced IR activity in the pH_2 solid, and propose this phenomenon as a diagnostic for H_2 molecules adsorbed by carbon nanotubes. C_{60}/pH_2 samples grown in an enclosed cell by laser ablation of solid C_{60} appear to contain predominantly $(C_{60})_n$ clusters; these clusters are too small to exhibit "bulk" vibrational or electronic properties, as determined by IR and UV/visible absorption spectroscopies. Future experiments to disentangle the contributions of ^{13}C isotopic substitution, pH_2 matrix effects, and the putative hindered rotation of C_{60} molecules to the observed C_{60}/pH_2 IR line shapes are presently under consideration.

I. Introduction

The fullerene literature has grown to over 15 000 publications,[1] encompassing early theoretical speculations[2] and predictions,[3] the mass spectrometric detection of buckminsterfullerene (C_{60}) and other fullerene molecules,[4,5] the production of macroscopic quantities of purified fullerenes,[6] the discovery of carbon nanotubes,[7,8] and a rapidly expanding number of more recent developments.[9−12] This profusion of activity reflects the diverse and multidisciplinary nature of fullerene research. In particular, the highly symmetrical truncated icosahedron C_{60} molecule has captured the imaginations of researchers in fields including: molecular spectroscopy, solid-state physics, interstellar chemistry, and materials science.

In this paper, we describe the application of high-resolution infrared (IR) absorption spectroscopy to the study of C_{60} molecules and clusters trapped in cryogenic parahydrogen (pH_2) solids. Improved spectroscopic data for the isolated C_{60} molecule could yield more precise knowledge of its equilibrium structure and rovibrational dynamics,[13−18] providing new benchmarks against which further improvements in theory could be measured; our ultimate goal is the observation and assignment of a rotationally resolved spectrum. Spectroscopic data on C_{60} van der Waals dimers and larger clusters in principle contain information about $C_{60}-C_{60}$ interactions, which could illuminate lattice vibrational and rotational dynamics in pure and doped C_{60} solids. Spectral features attributable to the presence of the pH_2 matrix host contain information about the structure(s) of the C_{60}/pH_2 trapping site(s) and the van der Waals interaction potential between C_{60} and H_2 molecules. An improved $C_{60}-H_2$ interaction potential could assist efforts to model the adsorption of H_2 by carbon nanotubes,[19−21] currently under investigation as a practical method for hydrogen fuel storage.

The theoretical groundwork for assigning a rotationally resolved electronic or vibrational spectrum of a low-temperature C_{60} sample has been well prepared.[13,14,22−26] However, despite the vastness of the fullerene literature, none of the reported experimental spectra show line widths or peak spacings characteristic of rotationally resolved features (vide infra). Gas phase IR emission measurements on samples at $T \approx 1000$ K reveal only ∼10 cm^{-1} full width at half-maximum (fwhm) unresolved bands.[27] The cold molecular beam electronic (resonant two-photon ionization, R2PI) spectrum of C_{60} at $T \sim 100$ K shows sharp vibronic features with line widths comparable to the 3 cm^{-1} experimental resolution.[28] The electronic absorption spectrum of C_{60} isolated in helium droplets[29] at $T \approx 0.4$ K shows lines as sharp as 1.5 cm^{-1} fwhm and is very similar to the molecular beam R2PI spectrum. Several reports of electronic absorption and emission spectra of C_{60} isolated in cryogenic rare gas matrices have appeared,[30−34] with no sign of rotational structure or peaks narrower than ∼10 cm^{-1} fwhm. These

† Part of the special issue "Marilyn Jacox Festschrift".

‡ E-mail: momose@kuchem.kyoto-u.ac.jp.
§ E-mail: mario_fajardo@ple.af.mil.

10.1021/jp9938718 CCC: $19.00
Published on Web 03/10/2000

vibronic features appear even less well resolved in electronic spectra of C_{60}/hydrocarbon solutions[35−39] and cryogenic glasses.[40] IR absorption studies of matrix-isolated C_{60} are badly underreported;[41] the narrowest line in this early C_{60}/Ar study is the 1 cm^{-1} fwhm $F_{1u}(1)$ absorption at 530.1 cm^{-1}. IR absorption[6,41−52] and Raman scattering[42,43,47,53−59] spectroscopies are widely employed as probes of C_{60} solids. The narrowest reported IR absorption feature is the 0.5 cm^{-1} fwhm $F_{1u}(2)$ absorption at 576.5 cm^{-1} in a 15 K solid C_{60} sample.[43] Raman spectra of C_{60} solids cooled to $T \approx 2$ K show much sharper fine structure,[55,58] with individual components having line widths as narrow as 0.1 cm^{-1}; the various features are sensitive to the samples' isotopic compositions and/or degree of orientational disorder. Vibrational transitions of C_{60} in liquid solutions[43,60−62] and in solid phase compounds[63−66] typically show line widths of ≈1 cm^{-1} fwhm, or larger.

The phenomenon of high-resolution IR spectroscopy in doped pH_2 solids was discovered by Oka and co-workers at the University of Chicago,[67] and further developed in collaboration with Shida, Momose, and co-workers at Kyoto University.[68−74] Two suggestive examples: line widths as narrow as 0.0003 cm^{-1} are observed for the $Q_1(0)$ transition of isolated D_2 molecules;[67] the ν_4 band of CH_4/pH_2 shows that the CH_4 molecules exist as very slightly hindered rotors, with rovibronic spectral features as narrow as 0.003 cm^{-1}.[71] The spherical nature of the ground state ($v = 0$, $J = 0$) pH_2 molecule, the weak attractive pH_2-pH_2 interactions, and the small H_2 mass all contribute to make solid pH_2 a very "soft" matrix host, reducing the incidence and importance of inhomogeneities in a guest molecule's environment. Recently, Fajardo and Tam at Edwards Air Force Base demonstrated the efficient isolation of various atomic and molecular dopants by rapid vapor deposition of the pH_2 solid.[75,76] In a recent collaborative study,[77] we demonstrated the combination of high-resolution IR spectroscopy and rapid vapor deposition of CH_4 doped pH_2 solids, obtaining very similar results to the previous CH_4/pH_2 study. This favorable outcome motivated the present investigation of the possibility of observing rotationally resolved spectra of C_{60} molecules isolated in solid pH_2.

In what follows, we report our *preliminary* results on the spectroscopy of C_{60}/pH_2 solids. We begin with theoretical predictions of possible rovibrational absorption spectra of isolated C_{60} molecules at liquid helium temperatures. We give a qualitative argument for the possibility of isolating C_{60} molecules in fairly small, high-symmetry trapping sites in the pH_2 solid: sites in which the C_{60} molecules might exist as slightly hindered rotors. We describe our experimental apparatus and procedures, and present the results of various spectroscopic measurements on C_{60}/pH_2 solids. *While we do not observe rotationally resolved spectra, we do report the narrowest IR absorption features for C_{60}, to date*. We discuss these results in the context of the issues raised above. Experiments to determine the influences of the ^{13}C isotopic composition of our C_{60} samples, of spectral perturbations induced by the pH_2 host, and of possible rotation of the trapped C_{60} molecules are still in progress. Accordingly, those results, and a detailed final analysis of our IR absorption line shapes, will be postponed until a later publication.

II. Theory

A. Rovibrational States of $^{12}C_{60}$. The buckminsterfullerene (C_{60}) molecule has a hollow-cage, nearly spherical shape with icosahedral (I_h) symmetry.[9−11] Because of this highly symmetrical structure, many of its physical and chemical properties are quite unique. For instance, among the 174 vibrational degrees of freedom, there are only 46 distinct vibrational frequencies, and only the 4 modes of F_{1u} symmetry are IR active.[23]

C_{60} is a spherical top rotor with a small rotational constant of $B \approx 0.0028$ cm^{-1}; thus, even at temperatures below 10 K a large number of rotational levels will be occupied. However, in the specific case of the $^{12}C_{60}$ molecule (i.e., all 60 carbon atoms are the ^{12}C isotope), boson-exchange symmetry restrictions require that many of the rotational quantum levels do not exist.[23] These predicted "missing" levels result in a characteristic pattern of spectral line spacings which we expect will be key to observing and assigning a rotationally resolved C_{60} spectrum. We will address the effects of ^{13}C isotopic substitutions in a subsequent section.

In $^{12}C_{60}$, all 60 carbon nuclei have zero spin. The total wave function $\Psi_{el}\Psi_{vib}\Psi_{rot}\Psi_{ns}$ must be invariant under any permutation of ^{12}C nuclei, where Ψ_{el}, Ψ_{vib}, Ψ_{rot} , and Ψ_{ns} denote the electronic, vibrational, rotational, and nuclear-spin wave functions, respectively. Since the molecule has one possible nuclear-spin wave function of A_g symmetry in the point group I_h, and since the IR absorption occurs in the ground electronic state of A_g symmetry, the rovibrational wave function $\Psi_{vib}\Psi_{rot}$ should have A_g or A_u symmetry.[78,79]

To find the allowed rotational levels satisfying these boson-exchange symmetry restrictions, it is convenient to consider irreducible representations in the pure rotational subgroup of I_h; that is, in I, where $I_h = I \otimes i$, with i being the inversion operation. Then the rovibrational wave function $\Psi_{vib}\Psi_{rot}$ should have A symmetry in I. In the case of the vibrational ground state where Ψ_{vib} has A_g symmetry in I_h, the possible rotational states Ψ_{rot} are those of A symmetry in I. Thus, the allowed rotational levels are only 1 level among each of $J = 0$, 6, 10, 12, 15, 16, 18, 20, 21, 22, 24−28, and 31−35; and 2 levels among each of $J = 30$ and 36 and so on.[23] The rotational levels of $J = 1-5$, 7−9, 11, 13, 14, 17, 19, 23, and 29 are all missing in the ground vibrational state. For example, in the case of $J = 5$ there are $2(5) + 1 = 11$ conceivable rotational levels having $F_1 \oplus F_2 \oplus H$ symmetry in I, but none of them is allowed in the vibrational ground state of $^{12}C_{60}$. On the other hand, in the case of the vibrationally excited states of F_{1u} symmetry, it is found that the allowed rotational levels are 1 level among each of $J = 1$, 5−7, 9, 10, 12−14, and 18; and 2 levels among each of $J = 11$, 15−17, and 19, and so on. The rotational levels of $J = 0$, 2−4, and 8 are all missing in the F_{1u} vibrational excited state. For example, $3(2(5) + 1) = 33$ levels are conceivable for $J = 5$ rovibrational levels; they have $F_1 \otimes (F_1 \oplus F_2 \oplus H) = A \oplus 2F_1 \oplus F_2 \oplus 2G \oplus 3H$ symmetry in I. Among them, only one rovibrational level with A symmetry is allowed for $^{12}C_{60}$.

The rovibrational Hamiltonian of $^{12}C_{60}$ is that of a spherical top molecule.[78] The ground state energies can be expressed as $BJ(J + 1)$, where J is the rotational quantum number. In the case of the triply degenerate F_{1u} vibrational excited states, the degeneracy is lifted into three levels due to the Coriolis coupling interaction. By denoting the vibrational, rotational, and total angular momenta as l, R, and $J = l + R$, respectively, the rovibrational energies of each level can be expressed as follows:[78]

$$F_{1u}^{(-)}(J) = \nu_{vib} + BJ(J+1) - 2B\zeta J \qquad \text{for } R = J - 1 \quad (1a)$$

$$F_{1u}^{(0)}(J) = \nu_{vib} + BJ(J+1) \qquad \text{for } R = J \quad (1b)$$

$$F_{1u}^{(+)}(J) = \nu_{vib} + BJ(J+1) + 2B\zeta(J+1) \qquad \text{for } R = J + 1 \quad (1c)$$

where ν_{vib} and ζ are the band origin and the Coriolis coupling constant, respectively. Note that the vibrational angular mo-

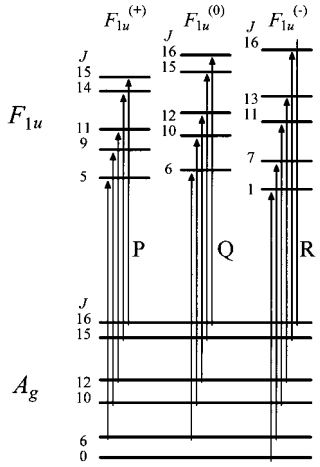

Figure 1. Schematic energy levels of the upper F_{1u} and lower A_g rovibrational states of $^{12}C_{60}$. Because of boson-exchange symmetry restrictions, many levels are missing; all allowed levels are shown up to $J = 16$. Only transitions that conserve the quantum number R are allowed resulting in P-, Q-, and R-branches, which are shown by arrows.

mentum of the F_{1u} state is $l = 1$. The magnitude and the sign of the Coriolis coupling constant ζ depend on the vibrational mode and should be determined experimentally, which is yet to be done. Calculated values[13] for the four F_{1u} modes of C_{60} are $\zeta_1 = -0.107$ for $F_{1u}(1)$ at 530 cm^{-1}, $\zeta_2 = -0.498$ for $F_{1u}(2)$ at 578 cm^{-1}, $\zeta_3 = -0.319$ for $F_{1u}(3)$ at 1184 cm^{-1}, and $\zeta_4 = -0.076$ for $F_{1u}(4)$ at 1432 cm^{-1}. Note that these values satisfy the relation $\sum\zeta_i(F_{1u}) = -1$. In Figure 1, the rotational energy levels for the upper F_{1u} and lower A_g vibrational states of $^{12}C_{60}$ are depicted with the assumption of $\zeta < 0$. The IR allowed transitions are also shown by arrows where the selection rule is $\Delta R = 0$. It is seen that the P branch is composed of the transitions to $F_{1u}^{(+)}$ levels, the Q branch to $F_{1u}^{(0)}$ levels, and the R branch to $F_{1u}^{(-)}$ levels, respectively.

The rotational population distribution $P(J)$ for a spherical top molecule at a given temperature T is proportional to the Maxwell−Boltzmann factor:[78]

$$P(J) \propto (2J + 1)g(J) \exp[-BJ(J + 1)hc/kT] \qquad (2)$$

The first term of the right-hand side, $2J + 1$, corresponds to the degeneracy of J projected along a space fixed axis. The second factor $g(J)$ corresponds to the degeneracy of J projected along a molecule fixed axis. Without the boson-exchange symmetry restrictions $g(J)$ is equal to $2J + 1$. However, as mentioned above, the boson-exchange symmetry restrictions requires that for the ground state of $^{12}C_{60}$ the factor should be $g(J) = 0$ for $J = 1-5, 7-9, 11, ...$; $g(J) = 1$ for $J = 0, 6, 10, ...$; $g(J) = 2$ for $J = 30, 36, 40, ...$, and so on. The relative intensities of the rovibrational absorption lines are calculated from the ground state population $P(J)$.

Figure 2 shows calculated spectral line shapes for an IR active transition $F_{1u} \leftarrow A_g$ of $^{12}C_{60}$ at $T = 5.0$ and 2.5 K. The rotational constant of $B = 0.0028$ cm^{-1} is assumed for both the upper F_{1u} and lower A_g vibrational states. The Coriolis coupling constant for the upper state is taken as $\zeta_3 = -0.319$, which is the calculated value[13] for the $F_{1u}(3)$ mode at 1184 cm^{-1}. The most obvious feature of this simulated spectrum is the very strong, sharp, overlapped Q-branch feature (see insets) which results from the assumption of equal rotational constants for upper and lower vibrational states. More revealing is the unevenly spaced pattern of rotational lines in the low-J portions of the P- and R-branches which reflects the missing rotational levels. At high-J regions a spacing of $\Delta = 2B(1 - \zeta) = 0.0074$ cm^{-1} is seen between adjacent spectral lines.

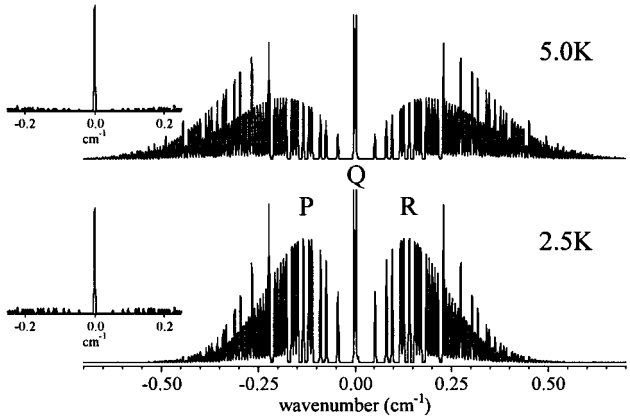

Figure 2. Simulated gas phase IR absorption line shape of the $F_{1u}(3) \leftarrow A_g$ transition of $^{12}C_{60}$ at $T = 5.0$ K (upper panel) and 2.5 K (lower panel). The rotational constant is $B = 0.0028$ cm^{-1} for both the upper and lower vibrational states, while the upper state Coriolis coupling constant is $\zeta_3 = -0.319$. The line width of each transition is assumed to be 0.0033 cm^{-1} (100 MHz) fwhm. The intensities of the Q-branch transitions are off-scale in the main figures; the insets show the spectra with the intensity of the Q-branch on-scale.

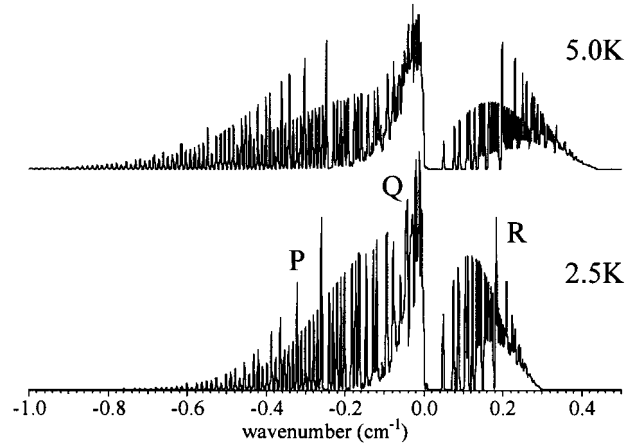

Figure 3. Simulated gas phase IR absorption line shape of the $F_{1u}(3) \leftarrow A_g$ transition of $^{12}C_{60}$ at $T = 5.0$ K (upper panel) and 2.5 K (lower panel). The calculation differs from the one depicted in Figure 2 only in that the rotational constant of the excited F_{1u} vibrational state is assumed to be 1% larger than in the ground state.

Figure 3 shows the results of a nearly identical pair of calculations, except that the rotational constant of the excited vibrational state is assumed to be 1% smaller than in the ground state. We expect this case to provide a comfortable upper limit to the actual anharmonic distortions experienced by a large molecule such as C_{60}, given only a single quantum of vibrational excitation. The corresponding increase in the C_{60} moment of inertia requires a radial enlargement by the cage of 0.5% (≈0.02 Å), and a 0.5% increase in all the C−C bond lengths (≈0.007 Å). We note in passing that such distortions have been considered before in simulations of C_{60} electronic spectra,[25] and of C_{70} rovibrational spectra.[27] Qualitatively, for nonzero anharmonic distortions the Q-branch transitions are not all coincident, and the missing level "null-gap" between the P- and Q-branches can be obliterated. However, for the R-branch the characteristic null gap and unevenly spaced rotational line pattern should survive intact.

Anticipating the possibility that individual rotational lines may not be resolved in a given experiment, Figure 4 shows the results of the same spectral simulations as in Figure 3, except at a degraded spectral resolution of 0.05 cm^{-1} fwhm. The band shapes are very similar to those calculated for C_{70} using

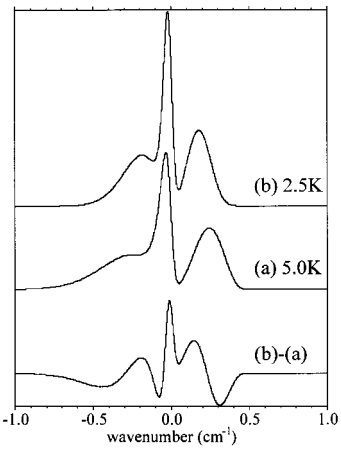

Figure 4. Simulated gas phase IR absorption line shape of the $F_{1u}(3) \leftarrow A_g$ transition of $^{12}C_{60}$ at (a) $T = 5.0$, (b) 2.5 K, and the difference spectrum (b) − (a). The calculation is identical to the one depicted in Figure 3, except that the spectral resolution has been degraded to 0.05 cm^{-1} fwhm.

comparable assumptions.[26] Note that the difference spectrum, trace (b) − (a), is plotted on the same vertical scale as the simulated spectra. Thus, in the absence of the direct observation of rotationally resolved features, we expect strong temperature induced changes to the rotational envelope over a ∼1 cm^{-1} region as a signature of rotating C_{60} molecules. We compare the results of this simulation directly to our experimental data, below.

B. ^{13}C Isotopic Substitution. In contrast to icosahedral $^{12}C_{60}$, the $^{13}C^{12}C_{59}$ molecule has only C_s symmetry,[23] and its rotational levels are those of a slightly prolate asymmetric top, without the strict bosonic-exchange exclusion.[23,24] The extra neutron also lifts the 3-fold degeneracy of the four F_{1u} vibrational modes[14] by amounts ranging from ≈0.5 to over 2 cm^{-1}. For $^{13}C_2^{12}C_{58}$, there are three possible symmetries: C_1, C_s, and C_{2v} occurring with probabilities 56/59, 1/59, and 2/59, respectively.[23] Thus, for the vast majority of $^{13}C_2^{12}C_{58}$ molecules, there are no symmetry restrictions on the rotational and vibrational states.[23]

The probabilities of a C_{60} molecule containing exactly n ^{13}C atoms is given by the Bernoulli Trials formula:[24]

$$P(p,n) = \frac{60!}{n!(60-n)!} p^n (1-p)^{60-n} \qquad (3)$$

For the natural ^{13}C isotopic abundance of $p = 0.011$, the relative concentrations of $^{12}C_{60}$, $^{13}C^{12}C_{59}$, and $^{13}C_2^{12}C_{58}$ are ≈0.51, 0.34, and 0.11, respectively. Thus, the experimental spectrum of a natural isotopic abundance C_{60} sample will be a superposition of the $^{12}C_{60}$, $^{13}C^{12}C_{59}$, and $^{13}C_2^{12}C_{58}$ spectra, weighted by their relative concentrations. This will seriously complicate the analysis of any vibrational spectrum, since nearly half of the C_{60} molecules will include at least one ^{13}C atom.

C. C_{60} Trapping Sites in Solid pH_2. Unlike the previously well-studied[70−72,77] example of CH_4/pH_2, the C_{60} molecule is far too large to fit into a single substitutional site in the pH_2 solid. We can estimate the size of the vacancy in solid pH_2 required to accommodate a C_{60} molecule as the ratio of the molecular volumes calculated according to

$$N_{vac} \approx \left(\frac{R_e(C_{60} - pH_2)}{R_{nn}(pH_2)} \right)^3 \qquad (4)$$

in which $R_e(C_{60}-pH_2)$ is the separation at the $C_{60}-pH_2$ potential minimum, and $R_{nn}(pH_2) \approx 3.79$ Å is the nearest-neighbor separation in solid pH_2 at liquid helium temperatures.[80] The use of $R_{nn}(pH_2)$ instead of $R_e(pH_2-pH_2)$ in eq 4 is intended to include quantum zero-point motion effects on the structure of solid pH_2, effects neglected in a simple potential energy minimization. This formula[81] for N_{vac} has yielded reasonable agreement with the results of Monte Carlo simulations of relaxed Li atom trapping sites in rare gas[82] and pH_2 solids.[83,84]

Unfortunately, we could not find a $C_{60}-pH_2$ van der Waals interaction potential in the literature, so we estimate $R_e(C_{60}-pH_2)$ by averaging[85] the minimum separations of the pH_2-pH_2 and $C_{60}-C_{60}$ interaction potentials:[80,86] $R_e(C_{60}-pH_2) \approx {}^1/_2\{R_e(C_{60}-C_{60}) + R_e(pH_2-pH_2)\} \approx {}^1/_2\{10.06\text{ Å} + 3.41\text{ Å}\} \approx 6.7$ Å. This value is in reasonable agreement with the sum of the radius of the C_{60} cage[86] and a typical adsorption separation for H_2 on graphite:[19] 3.55 Å + 2.95 Å = 6.5 Å. Thus, eq 4 predicts that a vacancy formed by removing approximately six pH_2 molecules is required to accommodate each C_{60} molecule.

Candidates for highly symmetrical 6-vacancies in close-packed pH_2 solids can be generated by removing the pH_2 molecules immediately surrounding the "octahedral" interstitial sites.[87] In face-centered cubic (fcc) solid pH_2, such a 6-vacancy site would have true O_h symmetry. However, in hexagonal close-packed (hcp) solid pH_2, which is anisotropic, the site symmetry is reduced to D_{3d}. Numerous other plausible trapping site structures of lower symmetry can be proposed. We simply note that the possibility of trapping C_{60} molecules in well defined, highly symmetrical sites encourages our expectations of sharp spectral features, and possibly even the existence of C_{60} molecules as slightly hindered rotors.

III. Experimental Section

Both experimental apparatus have been described in detail before;[68,69,71,73−77] here we give a brief summary, highlighting important modifications and additions.

A. Rapid Vapor Deposition. Doped pH_2 solids are prepared by rapid vapor deposition of precooled pH_2 gas and hot C_{60} vapor onto a CsI substrate cooled to $T \approx 2$ K in a lHe bath cryostat. We operate the ortho/para (o/p) converter at 15 K, with nH_2 (normal hydrogen) inlet rates between 25 and 50 mmol/h, yielding a flow of precooled 99.99% pH_2 which impinges upon the substrate at a 45° angle. During deposition the pressure of uncondensed pH_2 gas remains below ∼10^{-4} Torr. The C_{60} dopant (Aesar 99.5%) is vaporized in a stainless steel Knudsen oven[88] operated at temperatures between 820 and 850 K, resulting in C_{60} vapor pressures[89−92] of ∼10^{-2} Torr. Higher oven temperatures are avoided in order to minimize chemical reaction of the C_{60} with the uncondensed H_2 gas.[93] The 1.5 mm diameter oven orifice is situated 5 cm from the center of the CsI substrate at an angle of 45° from the substrate surface normal, at 90° to the pH_2 source.

We record IR absorption spectra of our C_{60}/pH_2 samples at resolutions of 0.1 and 0.01 cm^{-1} along the substrate normal. The FTIR spectrometer (Bruker IFS120HR) is equipped with a glowbar source, a KBr beam splitter, and three detectors: InSb (1800−9000 cm^{-1}), HgCdTe (550−7900 cm^{-1}), and a Si bolometer (400−700 cm^{-1}). Visible absorption spectra are recorded using a tungsten filament lamp source, and an optical multichannel analyzer equipped with an intensified silicon diode array detector mounted on a 275 mm focal length triple grating polychromator. The instrumental line width is ≈0.8 nm fwhm as measured using the Hg lamp calibration lines. To accommodate the IR diagnostic, the liquid He cryostat resides inside a 0.5 m^3 polycarbonate box purged with a constant flow of dry N_2 gas.

B. Enclosed Cell Condensation. C_{60}-doped pH_2 solids are prepared by cocondensation in an enclosed cell, as reported previously.[73,77] Normal hydrogen (nH_2) gas is converted to pure pH_2 in advance and kept in a tank at room temperature. The pH_2 gas is introduced through a thin stainless steel inlet tube into a copper cell cooled by a liquid helium (lHe) bath cryostat; the inlet gas flow rate is typically ≈300 mmol/h. C_{60} is volatilized inside the copper cell by pulsed laser ablation.[69] A 15 mm diameter by 2 mm thick solid C_{60} target disk is formed by pressing C_{60} powder onto an aluminum plate at $P \sim 20$ kgw/cm^2. During the pH_2 condensation, a pulsed laser beam from a Nd:YLF laser (Spectra Physics TFR: $\lambda = 523.5$ nm, ≈ 0.2 mJ/pulse, 1 kHz repetition rate) is focused on the surface of the C_{60} target using a 10 cm focal length lens.

The copper sample cell has an inner diameter of 2 cm and an optical path length of 3.0 cm with BaF_2 windows at both ends sealed with indium gaskets. The temperature of the sample cell is kept around 8.5 K during the 1.5 h long sample preparation. The sample is then cooled to 4.5 K for observation. The doped pH_2 solid grows radially inward from the cell walls and forms a polycrystalline aggregate of hcp crystals having their *c*-axes normal to the wall of the cell.[67,73] The sample thus grown is completely transparent.

IR absorption spectra are obtained with a Fourier transform infrared (FTIR) spectrometer (Bruker IFS120HR). A glowbar source, a KBr beam splitter, and a liquid nitrogen (lN_2) cooled HgCdTe detector, are employed to acquire spectra at resolutions of 0.25 and 0.01 cm^{-1}. UV/visible absorption spectra were recorded using a vacuum UV spectrometer (Jasco VUV-1C, 180−350 nm) and a visible spectrometer (Spex model 1680, 350−820 nm) with a spectral resolution of ≈ 0.2 nm.

IV. Results and Discussion

A. Isolated C_{60} Molecules. Figures 5−8 show absorption spectra of the four dipole allowed F_{1u} vibrational modes of C_{60} molecules isolated in rapid vapor deposited pH_2 solids. The C_{60} concentrations are estimated as ≈100 ppm, assuming a value for the integrated absorption coefficient of the $F_{1u}(3)$ mode of $\int \alpha(\bar{\nu})\, d\bar{\nu} = 25$ km/mol.[15,94] The samples also contain ∼1 ppm of H_2O and CO_2 as contaminants. In each figure, trace (a) is for the as-deposited sample at $T = 2.4$ K, trace (b) is for the sample warmed to $T = 4.8$ K, and trace (c) is for the "annealed" sample cooled back to $T = 2.4$ K. *To the best of our knowledge, the ≈0.2 cm^{-1} fwhm peaks in the spectra of the $F_{1u}(1)$ mode constitute the sharpest IR absorption features ever reported for the C_{60} molecule.*

The difference traces in Figures 5−8 labeled "(c) − (a)" show the effects of the complete "annealing" temperature cycle, corresponding to irreversible changes in the environments of the C_{60} molecules, e.g.: C_{60} clustering and/or changes to the pH_2 host. Our previous experiments on pure,[75] and 10−100 ppm CH_4 doped,[77] rapid vapor deposited pH_2 solids have demonstrated that the as-deposited samples have a mixed fcc/hcp structure which anneals nearly completely to hcp upon warming to $T \approx 5$ K. This conversion is accompanied by pronounced changes to the rovibrational spectrum of the trapped CH_4 molecules.[77] In the present case of ∼100 ppm C_{60}/pH_2 samples, the annealing process appears ineffectual, with very little resulting changes to the absorption line shapes.

Not shown are spectra of the CH_4 ν_4 band region for another C_{60}/pH_2 sample produced using a higher Knudsen oven temperature; the CH_4 (∼1 ppm) is presumably produced in the Knudsen oven by reactions with uncondensed pH_2 gas. Annealing of that sample failed to induce the expected fcc to hcp transformation, as revealed by the CH_4 spectroscopy. The fcc to hcp conversion most likely proceeds by the relative slipping motion of adjacent close-packed planes. Apparently the CH_4 molecules, which fit into single substitutional sites, do not hinder this process, whereas the larger C_{60} molecules, which intrude into adjacent close-packed planes, inhibit their relative motion. The presence of residual inhomogeneous line broadening due to the mixed fcc/hcp structure implies that even sharper spectral features may be obtainable in C_{60}/pH_2 solids prepared under different conditions.

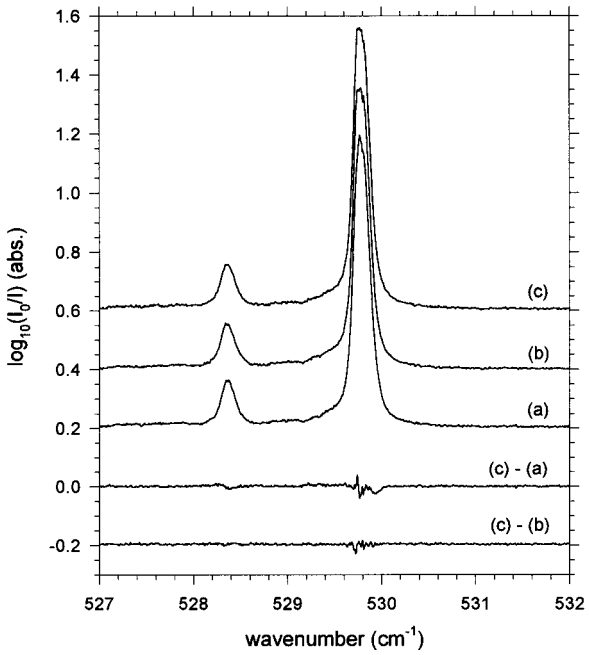

Figure 5. IR absorption spectrum (resolution = 0.01 cm^{-1}) of $F_{1u}(1)$ mode in rapid vapor deposited C_{60}/pH_2. Trace (a) is for the as-deposited sample at 2.4 K, (b) warmed to 4.8 K, (c) recooled to 2.4 K, (c) − (a) effects of annealing, (c) − (b) effects of final cooldown. The sample remains at each temperature for 1 h. During the 30 min long sample deposition the Knudsen oven temperature is 820(±10) K and the pH_2 inlet rate is 25 mmol/h (sample thickness growth rate ≈ 7 μm/min). The final C_{60} concentration is estimated as 100 ppm, and the sample thickness as 0.2 mm.

The difference traces in Figures 5−8 labeled "(c) − (b)" show the effects of cooling the samples back down from 4.8 to 2.4 K. We expect these difference traces to include signs of both irreversible and reversible changes to the samples, i.e.: the final phases of the annealing process, and any possible temperature-induced changes to the C_{60} rotational state populations. Unfortunately, during these experiments we were unable to complete a second temperature cycle to isolate the reversible temperature dependence completely.

Nonetheless, the qualitative resemblance between the simulated spectra and difference trace in Figure 4, vs the experimental data for the $F_{1u}(2)$ and $F_{1u}(3)$ modes in Figures 6 and 7, supports the notion that some fraction of the C_{60} molecules may exist as slightly hindered rotors. However, the relatively small magnitudes of the thermally induced changes in the experimental spectra, as compared to the large effects predicted by the simulations, implies that at most only a small fraction of the C_{60} molecules can rotate. Further constraining this interpretation is the narrow (0.2 cm^{-1} fwhm) line width and apparent temperature *independence* of the $F_{1u}(1)$ mode shown in Figure 5, for which the expected P- and R-branches are not apparent. This spectrum implies that *none* of the C_{60} molecules are capable of rotating.

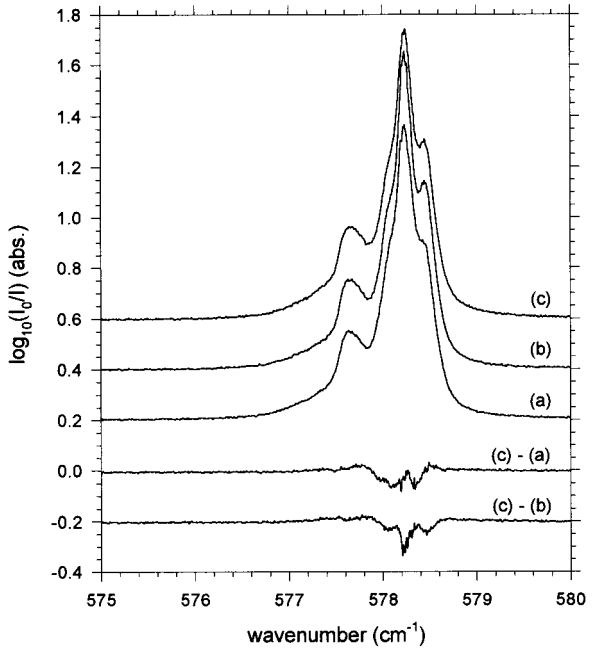

Figure 6. IR absorption spectrum (resolution = 0.01 cm^{-1}) of $F_{1u}(2)$ mode in rapid vapor deposited C_{60}/pH_2. Trace (a) is for the as-deposited sample at 2.4 K, (b) warmed to 4.8 K, (c) recooled to 2.4 K, (c) − (a) effects of annealing, (c) − (b) effects of final cooldown. The sample remains at each temperature for 1 h. During the 70 min long sample deposition the Knudsen oven temperature is 850(±10) K and the pH_2 inlet rate is 50 mmol/h (sample thickness growth rate ≈ 14 μm/min). The final C_{60} concentration is estimated as 110 ppm, and the sample thickness as 1.0 mm.

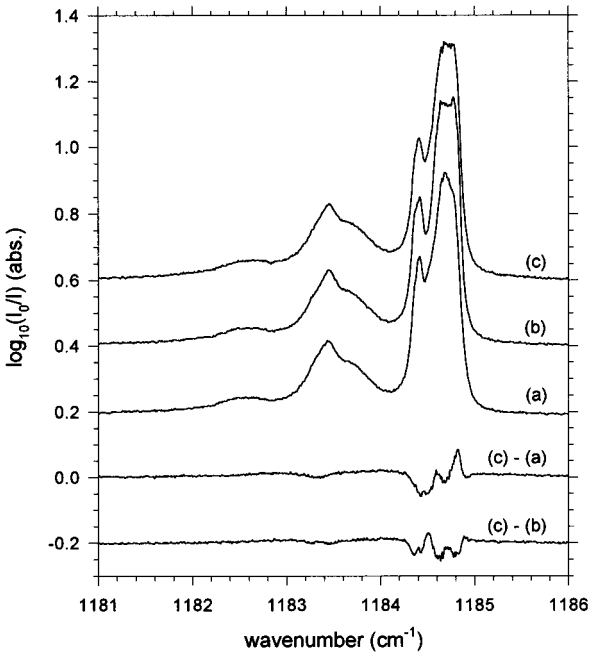

Figure 7. IR absorption spectrum of $F_{1u}(3)$ mode in rapid vapor deposited C_{60}/pH_2. Sample preparation and interrogation are described in the caption to Figure 6.

Clearly, thermally induced rotational population changes, and the slightly hindered rotor C_{60} molecules they imply, cannot be completely ruled out given the present data. A final determination of the influences of ^{13}C isotopic substitution, pH_2 matrix effects, and the C_{60} rotational state distribution on the observed C_{60}/pH_2 band shapes awaits further experimentation and analysis. We are preparing to conduct a new study involving the deposition of ^{13}C depleted and enriched C_{60} into various cryogenic matrix hosts using a range of different deposition conditions. Any informative results will be published at a later time.

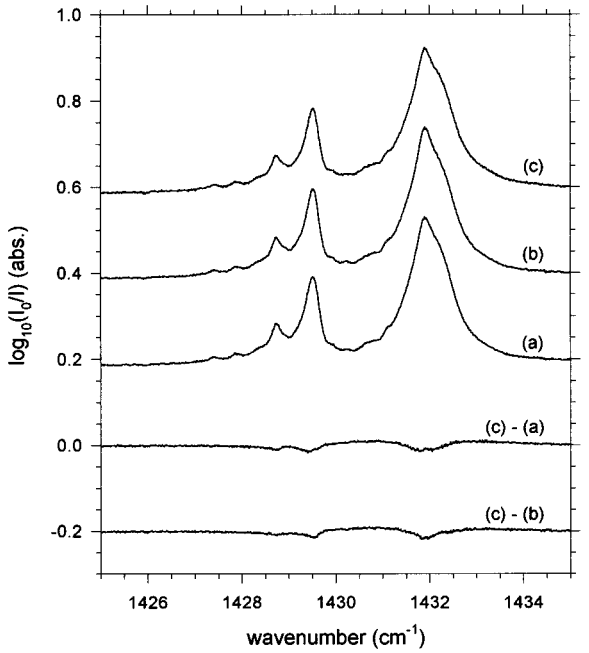

Figure 8. IR absorption spectrum of $F_{1u}(4)$ mode in rapid vapor deposited C_{60}/pH_2. Sample preparation and interrogation are described in the caption to Figure 6.

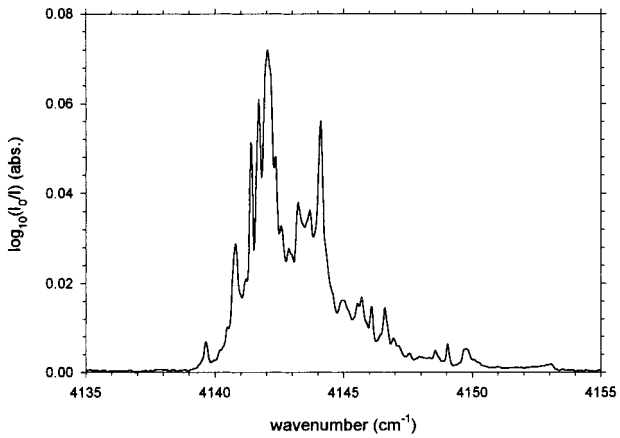

Figure 9. IR absorption spectrum (resolution = 0.1 cm^{-1}) of the pH_2 $Q_1(0)$ dopant-induced feature in rapid vapor deposited C_{60}/pH_2. Sample preparation conditions are described in the caption to Figure 6.

In addition to the direct dopant IR absorptions, dopant-induced IR features are observed in our C_{60}/pH_2 samples, as shown in Figure 9. The best known example of this phenomenon is the $Q_1(0)$ line at 4153 cm^{-1} induced by oH_2 impurities.[75,76,95−97] We have observed similar dopant induced IR activity for a number of atomic and molecular dopant species.[75,98] A general model for assigning these spectra is still being developed. However, the complexity of the induced IR spectra appears to increase in the following dopant sequence: atomic, diatomic, polyatomic, perhaps reflecting the increasing number of dissimilar environments, and hence Stark shifts, experienced by the participating pH_2 molecules. If so, the complexity of the C_{60}-induced spectrum implies a large number of dissimilar environments for the surrounding pH_2 molecules. Any "complete" model of C_{60}/pH_2 trapping site structure(s) would have to explain these data as well as the direct IR absorption line shapes.

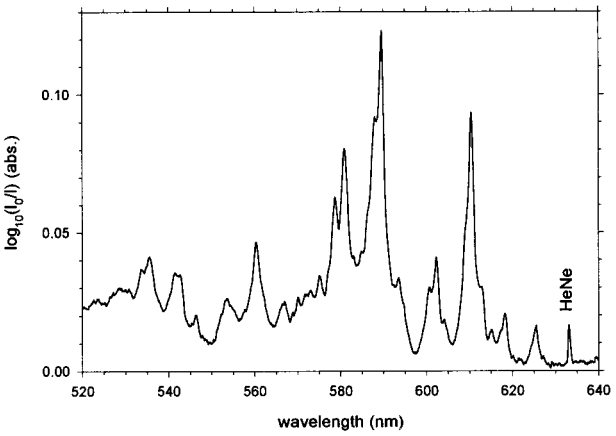

Figure 10. Visible absorption spectrum (resolution = 0.8 nm) of a C_{60}/pH_2 solid. Sample preparation conditions are described in the caption to Figure 6. The peak marked "HeNe" is due to scattered HeNe laser light and shows the instrumental resolution.

We note that the total integrated intensity of the induced IR spectrum is comparable in magnitude to that of the direct C_{60} absorptions; we estimate $\int \alpha_{ind}(\bar{\nu})\, d\bar{\nu} \approx 7$ km/mol, where the corresponding concentration is that of the C_{60} dopant.[94] Thus, we propose this induced IR phenomenon as a diagnostic for probing the chemical environments of pH_2 molecules adsorbed by carbon nanotubes at cryogenic temperatures. If experimental conditions can be arranged to observe the nanotube IR absorptions, then we predict that the nanotube-induced IR activity in the adsorbed pH_2 molecules should also be measurable. This technique has recently been applied to characterize the electric fields experienced by H_2 molecules adsorbed in zeolites.[99]

Figure 10 shows a portion of the visible absorption spectrum of the as-deposited C_{60}/pH_2 sample depicted in Figures 6−8. The spectral features are similar to, but somewhat broader than, those observed in previous molecular beam,[28] helium droplet,[29] and Ne matrix studies.[33,34] The observed spectral line widths do not appear to be limited by the ≈0.8 nm (≈20 cm^{-1}) experimental resolution. The sharp peaks observed in this spectrum further support our assignment of the spectra presented in this section to isolated C_{60} molecules.

B. C_{60} Clusters. Solid pH_2 samples produced by the enclosed cell condensation method have a predominantly hcp microscopic structure.[67,73] Consequently, inhomogeneities in dopant molecule environments should be reduced in cell condensed doped pH_2 samples, an important advantage over rapid vapor deposited samples which are mixed fcc and hcp. For example, the line widths of the ν_4 CH_4 absorptions in cell condensed CH_4/pH_2 samples are measurably smaller than in annealed rapid vapor deposited samples.[77] Unfortunately, the same elevated sample preparation temperature which leads to formation of the thermodynamically stable pure hcp phase also results in greatly increased clustering of the dopant molecules.

Figure 11 shows an IR absorption spectrum of laser vaporized C_{60} trapped in solid pH_2 grown in an enclosed cell. The peaks at 1184.3 and 1431.8 cm^{-1} are identified as the $F_{1u}(3)$ and $F_{1u}(4)$ IR active fundamentals of C_{60}, respectively. The strong peak at 1167.1 cm^{-1}, and the broad band ranging from 1200 to 1500 cm^{-1}, are due to the $U_0(0)$ transition of solid pH_2 and its phonon sideband, respectively.[100] The sharp peak at 1308 cm^{-1} corresponds to the ν_4 mode of CH_4. Not shown is a sharp peak at 2034.4 cm^{-1} which is due to the ν_3 mode[69] of C_3. These smaller carbon-containing species are formed by photofragmentation of the C_{60} by the ablation laser, and, in the case of CH_4, by subsequent reactions with the pH_2 host. The sharp spikes in the

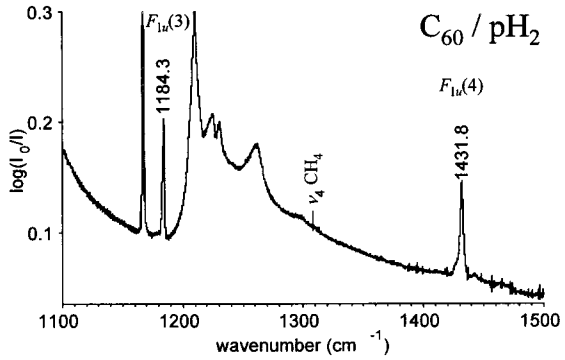

Figure 11. IR absorption spectrum (resolution = 0.25 cm^{-1}) of a C_{60}/pH_2 sample grown in an enclosed cell by laser ablation of C_{60}.

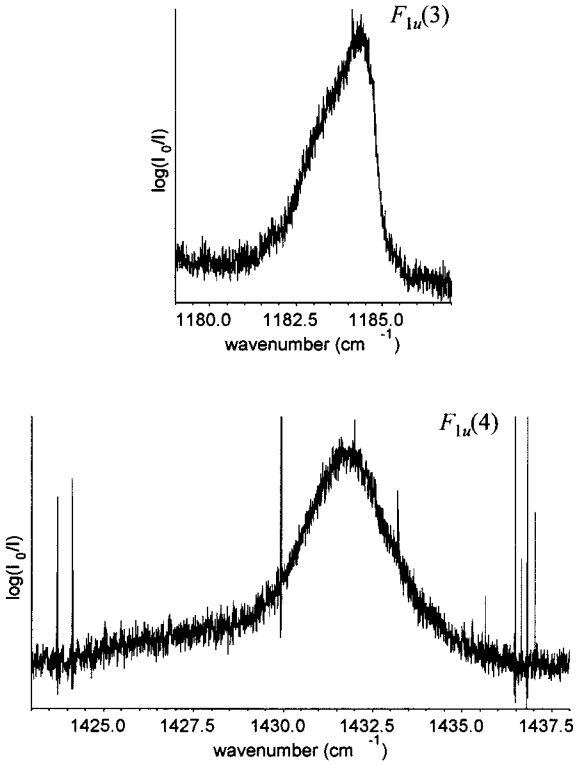

Figure 12. IR absorption spectra of the $F_{1u}(3)$ and $F_{1u}(4)$ modes of a C_{60}/pH_2 solid grown in an enclosed cell; resolution = 0.01 cm^{-1}. Sharp spikes in the spectra are due to inexact cancellation of absorptions by water in the laboratory air.

1380 to 1500 cm^{-1} region are due to inexact cancellation of absorptions by water vapor in the laboratory air.

Figure 12 shows the absorption line shapes of the $F_{1u}(3)$ and $F_{1u}(4)$ modes in greater detail, recorded at a higher resolution of 0.01 cm^{-1}. The spectrum of the $F_{1u}(3)$ mode consists of two components: one peaking at 1184.3 cm^{-1}, and a shoulder at 1183.2 cm^{-1}. The spectrum of $F_{1u}(4)$ is more difficult to deconvolve into multiple components, but shows signs of a long red-degraded tail. Both spectra appear to be broadened versions of the C_{60} monomer $F_{1u}(3)$ and $F_{1u}(4)$ mode spectra presented above in Figures 7 and 8. The additional line broadening is probably due to a higher extent of clustering of the C_{60} molecules in the enclosed cell grown sample.

The spectral peak positions and line widths observed for both the rapid vapor deposited, and enclosed cell grown C_{60}/pH_2 samples, are collected in Table 1, along with other values gleaned from the literature. The two sets of C_{60}/pH_2 data agree well with each other, and for the most part with the peak positions reported for a C_{60}/Ar sample[41] at $T = 10$ K (except

TABLE 1: Absorption Peaks (cm^{-1}) and Widths (fwhm) for the Four IR Allowed F_{1u} Vibrational Modes of C_{60} in (a) Annealed Rapid Vapor Deposited C_{60}/pH_2 Samples, and (b) Enclosed Cell Grown C_{60}/pH_2 Samples[a]

	this study		literature					
mode	C_{60}/pH_2 2.4 K (a)	C_{60}/pH_2 5 K (b)	C_{60}/Ar 10 K [41]	C_{60} film 15 K [43]	C_{60} film 80 K [50, 51]	C_{60} film 300 K [43]	C_{60} film 300 K [50, 51]	C_{60}/CS_2 300 K [43]
$F_{1u}(1)$	528.37 (0.18)							
	529.77 (0.20)	n.o.	530.1 (1)	525.5 (1.6)	525.7 (2.6)	526.2 (2.7)	526.4	527.9 (2.6)
	533.6 w (0.3)							
$F_{1u}(2)$	577.6 (0.3)							
	578.05 sh							
	578.24 (0.3)	n.o.	579.3 (2)	576.5 (0.5)	576.4 (1.0)	576.1 (1.9)	575.5	577.8 (1.9)
	578.45 sh							
$F_{1u}(3)$	1182.6 w (0.5)							
	1183.45 (0.5)							
	1184.41 (0.1)	1184.3 (2.0)	1184.8 (2)	1183.7 (1.9)	1183.6 (2.0)	1183.0 (3.1)	1183.0	1182.9 (2.8)
	1184.7 (0.3)							
$F_{1u}(4)$	1427.4 w (0.2)							
	1427.9 w (0.2)							
	1428.7 (0.2)			1424.4 (1.2)	1424			
	1429.5 (0.3)			1428.4 (1.2)	1428			
	1431.9 (1.0)	1431.8 (2.5)	1431.9 (4)	1432.3 (3.1)	1432	1429.8 (4.0)	1429.5	1429.1 (3.4)
	1432.3 sh							

[a] Peak positions and widths from the literature are included for comparison (references given in square brackets). sh = shoulder; w = weak intensity; n.o. = not observable.

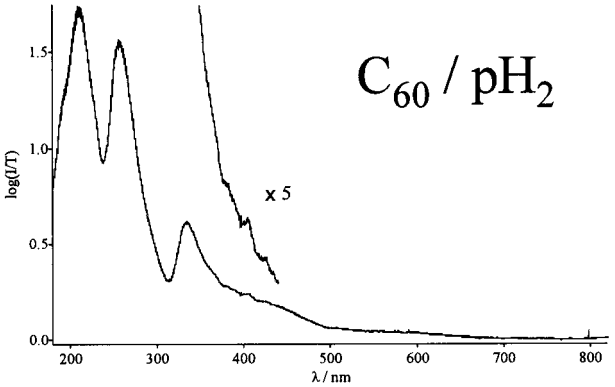

Figure 13. UV/visible absorption spectrum of a C_{60}/pH_2 solid grown in an enclosed cell.

for the $F_{1u}(2)$ mode which shows a discrepancy of about 1.0 cm^{-1}). However, the C_{60}/pH_2 peak positions and qualitative line shapes do *not* agree well with the solid C_{60} data, even for solid C_{60} temperatures below the orientational glass transition temperature[51] of ≈90 K. Specifically, the position of the $F_{1u}(3)$ mode peak, and the number of peaks observed for the $F_{1u}(4)$ mode, are different for enclosed cell grown C_{60}/pH_2 solids and low-temperature C_{60} films. These results show that the $(C_{60})_n$ clusters in the C_{60}/pH_2 sample are too small to exhibit "bulk" solid C_{60} vibrational behavior.

Figure 13 shows a UV/visible absorption spectrum of the enclosed cell grown C_{60}/pH_2 sample. The spectrum is dominated by three bands peaking at 211, 257, and 334 nm, followed by a broad hump ranging in the 380−500 nm region. A relatively narrow absorption feature at 405 nm is superimposed on this broad hump (see the inset in Figure 13). A tailing absorption starting near 500 nm spans up to 700 nm. (Note that the absorption intensities below ≈250 nm should not be compared quantitatively with other regions because of significant wavelength-dependent light scattering by the solid.)

The main bands at 211, 257, and 334 nm in Figure 13 are identified as dipole-allowed electronic transitions of C_{60}; similar bands have been reported for both C_{60} in solution[35,36] and for thin films[6] of solid C_{60}. Isolated C_{60} also exhibits two sharp peaks at around 405 nm separated by ≈4 nm, as has been observed for isolated C_{60} in the gas phase,[28] in solution,[36] and in cold matrices.[28,36] However, the absorption at 405 nm in Figure 13 has only one peak with a much broader line width than expected for isolated C_{60}. Moreover, the broad hump in the 380−500 nm region is a characteristic feature of C_{60} thin films[6] but not of C_{60} in solution.[35,36] Therefore, the observation of the hump in Figure 13 indicates that the C_{60} molecules in the enclosed cell grown sample are not completely isolated. Finally, the structureless tailing absorption in the 500−700 nm region seen in Figure 13 is not compatible with the structure-rich spectra observed for isolated C_{60} at low temperatures,[28,29,34] as typified by the C_{60}/pH_2 spectrum in Figure 10.

One might expect that the absorption feature at 405 nm corresponds to the well-known cometary band[101] of C_3. The electronic absorption of C_3 isolated in solid pH_2 was recently observed in Kyoto; it appears at 408 nm and has quite sharp line widths of ≈0.8 cm^{-1} fwhm.[102] The broad absorption feature at 405 nm in Figure 13 is clearly different from the observed

electronic absorption of C_3. Therefore, we conclude that the 405 nm band originates from C_{60}.

Both the IR and UV/visible observations indicate that C_{60} molecules are not well isolated in the enclosed cell grown C_{60}/pH_2 sample. However, the spectroscopy does not match that expected for cryogenic bulk C_{60}, either. A natural interpretation is that the laser ablation process produces $(C_{60})_n$ clusters that are trapped intact in the matrix. Cluster beams of $(C_{60})_n$ are reported by mass spectroscopy of laser vaporized thin films of C_{60} in a supersonic helium-gas expansion source.[103] Even under vacuum, laser ablation of C_{60} results in coalescence of the molecules to give higher mass peaks of $(C_{60})_n^+$.[104,105]

Thus, it appears that in this instance the spectral broadening due to C_{60} cluster formation overwhelms the inherent advantage of pure hcp solid pH_2 structure formation, resulting in broader observed lines for enclosed cell grown samples than for rapid vapor deposited samples.

V. Summary and Future Directions

We have performed theoretical simulations of rotationally resolved rovibrational spectra of isolated C_{60} molecules at liquid helium temperatures, including the effects of boson-exchange symmetry restrictions on the rotational levels of the icosahedral $^{12}C_{60}$ molecule. The simulations predict a characteristic "null gap" and unequal rotational line spacings for low-J values as a consequence of the symmetry forbidden missing rotational levels.

We have successfully isolated C_{60} molecules in cryogenic pH_2 solids using the rapid vapor deposition sample preparation method. High-resolution IR absorption spectra of these samples fail to show rotationally resolved features, and suggest that the majority of the C_{60} molecules cannot rotate. However, spectra of the $F_{1u}(1)$ vibrational mode show peaks with line widths of $\approx$0.2 cm^{-1} fwhm, the sharpest IR absorption bands for C_{60} reported to date. Visible absorption spectra show sharp features in the $\approx$600 nm region, supporting our contention that the C_{60} molecules are well isolated.

The presence of the C_{60} molecules in the pH_2 solid appears to inhibit the fcc to hcp conversion typically observed upon annealing to $T \approx 5$ K. We propose that this is due to the multisubstitutional nature of the C_{60} trapping site; the large guest molecule protrudes into adjacent close-packed planes and precludes their relative slipping motion. Efforts to generate sharper C_{60}/pH_2 IR absorptions should thus focus on the initial sample preparation phase, rather than on postdeposition processing.

We have observed IR absorptions of the pH_2 molecules induced by the presence of the C_{60} molecules. We are thus encouraged to continue our efforts to better understand $C_{60}-pH_2$ and more general fullerene$-H_2$ interactions. The integrated absorption strength of the induced feature is comparable to those of the direct C_{60} IR absorptions. We propose that this phenomenon can be used as a diagnostic of the chemical environments experienced by hydrogen molecules adsorbed by carbon nanotubes at cryogenic temperatures.

C_{60}/pH_2 samples grown in an enclosed cell by laser ablation of solid C_{60} appear to contain predominantly $(C_{60})_n$ clusters, as determined by IR and UV/visible absorption spectroscopies. These clusters are of insufficient size to exhibit true "bulk" vibrational and electronic spectra, yet still large enough to result in considerable line broadening as observed for the $F_{1u}(3)$ and $F_{1u}(4)$ modes. Our previous experience with $(CH_4)_n$ clusters in pH_2 suggests that high-resolution laser spectroscopic techniques may be capable of resolving sharp spectral features overlaying the broad IR absorption peaks.[72] Spectra of $(C_{60})_n$ clusters in solid pH_2 should ultimately yield important information about the $C_{60}-C_{60}$ interactions.

We have not disentangled the contributions of ^{13}C isotopic substitution, pH_2 matrix effects, and the putative hindered rotation of C_{60} molecules to the observed C_{60}/pH_2 IR line shapes. We are preparing for matrix isolation experiments on ^{13}C depleted and enriched C_{60} samples in a variety of matrix hosts. We hope that ultimately these efforts will illuminate the structure and vibrational dynamics of the C_{60} molecule via the observation of a rotationally resolved rovibrational spectrum.

Acknowledgment. The study in Kyoto was partially supported by Grant-in-Aid for Scientific Research of the Ministry of Education, Science, Culture and Sports of Japan. The authors thank Dr. J. A. Sheehy for a critical reading of the manuscript. We thank the reviewers for helpful comments concerning the magnitudes of anharmonic distortions to the C_{60} structure upon vibrational excitation, and the C_3 cometary band electronic spectrum.

References and Notes

(1) Chemical Abstracts Service, American Chemical Society.
(2) Jones, D. E. H. (*Daedalus*) *New Scientist* **1966**, *32*, 245; see also discussion in: Kroto, H. *Science* **1988**, *242*, 1139.
(3) Osawa, E. *Kagaku (Kyoto)* **1970**, *25*, 854; in Japanese.
(4) Rohlfing, E. A.; Cox, D. M.; Kaldor, A. *J. Chem. Phys.* **1984**, *81*, 3322.
(5) Kroto, H. W.; Heath, J. R.; O'Brien, S. C.; Curl, R. F.; Smalley, R. E. *Nature* **1985**, *318*, 162.
(6) Kratschmer, W.; Lamb, L. D.; Fostiropoulos, K.; Huffman, D. R. *Nature* **1990**, *347*, 354.
(7) Iijima, S. *Nature* **1991**, *354*, 56.
(8) Iijima, S.; Ichihashi, T. *Nature* **1993**, *363*, 603.
(9) McLafferty, F. W. *Acc. Chem. Res.* **1992**, *25*, 97; Special Issue on Buckminsterfullerenes.
(10) Dresselhaus, M. S.; Dresselhaus, G.; Eklund, P. C. *Science of Fullerenes and Nanotubes*; Academic Press: New York, 1996; ISBN 0-12-221820-5.
(11) Leach, S. *J. Phys. B* **1996**, *29*, 4855; Special Issue on Fullerenes: Atomic, Molecular and Optical Physics.
(12) Ebbesen, T. W. *Carbon Nanotubes: Preparation and Properties;* CRC Press: Boca Raton, FL, 1997.
(13) Weeks, D. E.; Harter, W. G. *Chem. Phys. Lett.* **1991**, *176*, 209.
(14) Weeks, D. E. *J. Chem. Phys.* **1992**, *96*, 7380.
(15) Dixon, D. A.; Chase, B. E.; Fitzgerald, G.; Matsuzawa, N. *J. Phys. Chem.* **1995**, *99*, 4486.
(16) Varga, F.; Nemes, L.; Watson, J. K. G. *J. Phys. B* **1996**, *29*, 5043.
(17) Negri, F.; Orlandi, G. *J. Phys. B* **1996**, *29*, 5049.
(18) Heid, R.; Pintschovius, L.; Godard, J. M. *Phys. Rev. B* **1997**, *56*, 5925.
(19) Dillon, A. C.; Jones, K. M.; Bekkedahl, T. A.; Kiang, C. H.; Bethune, D. S.; Heben, M. J. *Nature* **1997**, *386*, 377.
(20) Vidales, A. M.; Crespi, V. H.; Cole, M. W. *Phys. Rev. B* **1998**, *58*, R13426.
(21) Wang, Q.; Johnson, J. K. *J. Chem. Phys.* **1999**, *110*, 577.
(22) Harter, W. G.; Reimer, T. C. *Chem. Phys. Lett.* **1992**, *194*, 230.
(23) Saito, R.; Dresselhaus, G.; Dresselhaus, M. S. *Phys. Rev. B* **1994**, *50*, 5680.
(24) Reimer, T. C.; Harter, W. G. *J. Chem. Phys.* **1997**, *106*, 1326.
(25) Edwards, S. A.; Leach, S. *Astron. Astrophys.* **1993**, *272*, 533.
(26) Nemes, L. *J. Mol. Struct.* **1997**, *436*, 25.
(27) Frum, C. I.; Engleman, R., Jr.; Hedderich, H. G.; Bernath, P. F.; Lamb, L. D.; Huffman, D. R. *Chem. Phys. Lett.* **1991**, *176*, 504.
(28) Haufler, R. E.; Chai, Y.; Chibante, L. P. F.; Fraelich, M. R.; Weisman, R. B.; Curl, R. F.; Smalley, R. E. *J. Chem. Phys.* **1991**, *95*, 2197.
(29) Close, J. D.; Federmann, F.; Hoffmann, K.; Quaas, N. *Chem. Phys. Lett.* **1997**, *276*, 393.
(30) Gasyna, Z.; Schatz, P. N.; Hare, J. P.; Dennis, T. J.; Kroto, H. W.; Taylor, R.; Walton, D. R. M. *Chem. Phys. Lett.* **1991**, *183*, 283.
(31) Sassara, A.; Zerza, G.; Chergui, M. *Chem. Phys. Lett.* **1996**, *261*, 213.
(32) Hung, W. C.; Ho, C. D.; Liu, C. P.; Lee, Y. P. *J. Phys. Chem.* **1996**, *100*, 3927.
(33) Sassara, A.; Zerza, G.; Chergui, M. *J. Chem. Phys.* **1997**, *107*, 8731.

(34) Sassara, A.; Zerza, G.; Chergui, M.; Negri, F.; Orlandi, G. *J. Chem. Phys.* **1997**, *107*, 8731.
(35) Ajie, H.; Alvarez, M. M.; Anz, S. J.; Beck, R. D.; Diederich, F.; Fostiropoulos, K.; Huffman, D. R.; Kratschmer, W.; Rubin, Y.; Schriver, K. E.; Sensharma, D.; Whetten, R. L. *J. Phys. Chem.* **1990**, *94*, 8630.
(36) Leach, S.; Vervloet, M.; Despres, A.; Breheret, E.; Hare, J. P.; Dennis, T. J.; Kroto, H. W.; Taylor, R.; Walton, D. R. M. *Chem. Phys.* **1992**, *160*, 451.
(37) Catalan, J. *Chem. Phys. Lett.* **1994**, *223*, 159.
(38) Smith, A. L. *J. Phys. B* **1996**, *29*, 4975.
(39) Coheur, P. F.; Carleer, M.; Colin, R. *J. Phys. B* **1996**, *29*, 4987.
(40) van den Heuvel, D. J.; van den Berg, G. J. B.; Groenen, E. J. J.; Schmidt, J.; Holleman, I.; Meijer, G. *J. Phys. Chem.* **1995**, *99*, 11644.
(41) Haufler, R. E.; Conceicao, J.; Chibante, L. P. F.; Chai, Y.; Byrne, N. E.; Flanagan, S.; Haley, M. M.; O'Brien, S. C.; Pan, C.; Xiao, Z.; Billups, W. E.; Ciufolini, M. A.; Hauge, R. H.; Margrave, J. L.; Wilson, L. J.; Curl, R. F.; Smalley, R. E. *J. Phys. Chem.* **1990**, *94*, 8634.
(42) Bethune, D. S.; Meijer, G.; Tang, W. C.; Rosen, H. J.; Golden, W. G.; Seki, H.; Brown, C. A.; de Vries, M. S. *Chem. Phys. Lett.* **1991**, *179*, 181.
(43) Chase, B.; Herron, N.; Holler, E. *J. Phys. Chem.* **1992**, *96*, 4262.
(44) Fu, K. J.; Karney, W. L.; Chapman, O. L.; Huang, S. M.; Kaner, R. B.; Diederich, F.; Holczer, K.; Whetten, R. L. *Phys. Rev. B* **1992**, *46*, 1937.
(45) Huant, S.; Robert, J. B.; Chouteau, G.; Bernier, P.; Fabre, C.; Rassat, A. *Phys. Rev. Lett.* **1992**, *69*, 2666.
(46) Bini, R.; Procacci, P.; Salvi, P. R.; Schettino, V. *J. Phys. Chem.* **1993**, *97*, 10580.
(47) Horoyski, P. J.; Thewalt, M. L. W. *Phys. Rev. B* **1993**, *48*, 11446.
(48) Martin, M. C.; Du, X.; Kwon, J.; Mihaly, L. *Phys. Rev. B* **1994**, *50*, 173.
(49) Martin, M. C.; Fabian, J.; Godard, J.; Bernier, P.; Lambert, J. M.; Mihaly, L. *Phys. Rev. B* **1995**, *51*, 2844.
(50) Onoe, J.; Takeuchi, K. *J. Phys. Chem.* **1995**, *99*, 16786.
(51) Hara, T.; Onoe, J.; Takeuchi, K. *J. Phys. Chem. B* **1997**, *101*, 9532.
(52) Engeln, R.; von Helden, G.; van Roij, A. J. A.; Meijer, G. *J. Chem. Phys.* **1999**, *110*, 2732.
(53) Bethune, D. S.; Meijer, G.; Tang, W. C.; Rosen, H. J. *Chem. Phys. Lett.* **1990**, *174*, 219.
(54) Love, S. P.; McBranch, D.; Salkola, M. I.; Coppa, N. V.; Robinson, J. M.; Swanson, B. I.; Bishop, A. R. *Chem. Phys. Lett.* **1994**, *225*, 170.
(55) Horoyski, P. J.; Thewalt, M. L. W.; Anthony, T. R. *Phys. Rev. Lett.* **1995**, *74*, 194.
(56) Akselrod, L.; Byrne, H. J.; Donovan, S.; Roth, S. *Chem. Phys.* **1995**, *192*, 307.
(57) Horoyski, P. J.; Thewalt, M. L. W.; Anthony, T. R. *Phys. Rev. B* **1995**, *52*, R6951.
(58) Horoyski, P. J.; Thewalt, M. L. W.; Anthony, T. R. *Phys. Rev. B* **1996**, *54*, 920.
(59) Hadjiev, V. G.; Rafailov, P. M.; Jantoljak, H.; Thomsen, C.; Kelly, M. K. *Phys. Rev. B* **1997**, *56*, 2495.
(60) Tam, C. N.; Wang, B.; Keiderling, T. A.; Golden, W. G. *Chem. Phys. Lett.* **1992**, *198*, 123.
(61) Guha, S.; Menendez, J.; Page, J. B.; Adams, G. B.; Spencer, G. S.; Lehman, J. P.; Giannozzi, P.; Baroni, S. *Phys. Rev. Lett.* **1994**, *72*, 3359.
(62) Guha, S.; Menendez, J.; Page, J. B.; Adams, G. B. *Phys. Rev. B* **1997**, *56*, 15431.
(63) Swietlik, R.; Byszewski, P.; Kowalska, E. *Chem. Phys. Lett.* **1996**, *254*, 73.
(64) Graja, A.; Lapinski, A.; Krol, S. *J. Mol. Struct.* **1997**, *404*, 147.
(65) Paci, B.; Amoretti, G.; Arduini, G.; Ruani, G.; Shinkai, S.; Suzuki, T.; Ugozzoli, F.; Caciuffo, R. *Phys. Rev. B* **1997**, *55*, 5566.
(66) Long, V. C.; Musfeldt, J. L.; Kamaras, K.; Schilder, A.; Schutz, W. *Phys. Rev. B* **1998**, *58*, 14338.
(67) Oka, T. *Annu. Rev. Phys. Chem.* **1993**, *44*, 299.
(68) Momose, T.; Miki, M.; Uchida, M.; Shimizu, T.; Yoshizawa, I.; Shida, T. *J. Chem. Phys*. **1995**, *103*, 1400.
(69) Miki, M.; Wakabayashi, T.; Momose, T.; Shida, T. *J. Phys. Chem.* **1996**, *100*, 12135.
(70) Momose, T. *J. Chem. Phys.* **1997**, *107*, 7695.
(71) Momose, T.; Miki, M.; Wakabayashi, T.; Shida, T.; Chan, M. C.; Lee, S. S.; Oka, T. *J. Chem. Phys.* **1997**, *107*, 7707.
(72) Momose, T.; Katsuki, H.; Hoshina, H.; Sogoshi, N.; Wakabayashi, T.; Shida, T. *J. Chem. Phys.* **1997**, *107*, 7717.
(73) Momose, T.; Shida, T. *Bull. Chem. Soc. Jpn.* **1998**, *71*, 1.
(74) Hoshina, H.; Wakabayashi, T.; Momose, T.; Shida, T. *J. Chem. Phys.* **1999**, *110*, 5728.
(75) Fajardo, M. E.; Tam, S. *J. Chem. Phys.* **1998**, *108*, 4237.
(76) Tam, S.; Fajardo, M. E. *Rev. Sci. Instrum.* **1999**, *70*, 1926.
(77) Tam, S.; Fajardo, M. E.; Katsuki, H.; Hoshina, H.; Wakabayashi, T.; Momose, T. *J. Chem. Phys.* **1999**, *111*, 4191.
(78) Herzberg, G. *Molecular Spectra and Molecular Structure. Vol. II Infrared and Raman Spectra of Polyatomic Molecules*; Krieger Publishing: New York, 1991.
(79) Bunker, P. R.; Jensen, P.; *Molecular Symmetry and Spectroscopy*; NRC Research Press: Ottawa, 1998.
(80) Silvera, I. F. *Rev. Mod. Phys.* **1980**, *52*, 393.
(81) Fajardo, M. E. *J. Chem. Phys.* **1993**, *98*, 110.
(82) Fajardo, M. E. *J. Chem. Phys.* **1993**, *98*, 119.
(83) Scharf, D.; Martyna, G. J.; Li, D.; Voth, G. A.; Klein, M. L. *J. Chem. Phys.* **1993**, *99*, 9013.
(84) Cheng, E.; Whaley, K. B. *J. Chem. Phys.* **1996**, *104*, 3155.
(85) Maitland, G. C.; Rigby, M.; Smith, E. B.; Wakeham, W. A. *Intermolecular Forces*; Clarendon Press: Oxford, UK, 1981.
(86) Girifalco, L. A. *J. Phys. Chem.* **1992**, *96*, 858.
(87) Jackson, A. G. *Handbook of Crystallography*; Springer-Verlag: New York, 1991.
(88) Fajardo, M. E.; Carrick, P. G.; Kenney, J. W. III *J. Chem. Phys.* **1991**, *94*, 5812.
(89) Abrefah, J.; Olander, D. R.; Balooch, M.; Siekhaus, W. J. *Appl. Phys. Lett.* **1992**, *60*, 1313.
(90) Baba, M. S.; Narasimhan, T. S. L.; Balasubramanian, R.; Sivaraman, N.; Mathews, C. K. *J. Phys. Chem.* **1994**, *98*, 1333.
(91) Piacente, V.; Gigli, G.; Giustini, A.; Ferro, D. *J. Phys. Chem.* **1995**, *99*, 9, 14052.
(92) Berkowitz, J. *J. Chem. Phys.* **1999**, *111*, 1446.
(93) Han, K. L.; Lu, R. C.; Lin, H.; Gallogy, E. B.; Jackson, W. M. *Chem. Phys. Lett.* **1995**, *243*, 29.
(94) Fajardo, M. E.; Tam, S., unpublished data.
(95) Gush, H. P.; Hare, W. F. J.; Allin, E. J.; Welsh, H. L. *Can. J. Phys.* **1960**, *38*, 176.
(96) Van Kranendonk, J.; Karl, G. *Rev. Mod. Phys.* **1968**, *40*, 531.
(97) Van Kranendonk, J. *Solid Hydrogen*; Plenum Press: New York, 1983.
(98) Momose, T.; unpublished data.
(99) Stephanie-Victoire, F.; Cohen de Lara, E. *J. Chem. Phys.* **1998**, *109*, 6469.
(100) Chan, M. C.; Lee, S. S.; Okumura, M.; Oka, T. *J. Chem. Phys.* **1991**, *95*, 88.
(101) Herzberg, G. *Astrophys. J.* **1942**, ***96***, 314.
(102) Hoshina, H.; Morisawa, Y.; Kato, Y.; Wakabayashi, T.; Momose, T., to be submitted for publication
(103) Martin, T. P.; Naher, U.; Schaber, H.; Zimmermann, U. *Phys. Rev. Lett.* **1993**, *70*, 3079.
(104) Yeretzian, C.; Hansen, K.; Diederich, F.; Whetten, R. L. *Nature* **1993**, *359*, 44.
(105) Rao, A. M.; Zhou, P.; Wang, K. A.; Hager, G. T.; Holden, J. M.; Wang, Y.; Lee, W. T.; Bi, X. X.; Eklund, P. C.; Cornett, D. S.; Duncan, M. A.; Amster, I. J. *Science* **1993**, *259*, 955.